Cross-diffusion-induced subharmonic spatial resonances in a predator-prey system

G. Gambino[*] and M. C. Lombardo[†]
Department of Mathematics, University of Palermo, via Archirafi 34, 90123 Palermo, Italy

M. Sammartino[‡]
DIID, University of Palermo, Viale delle Scienze, Ed. 8, 90128 Palermo, Italy

(Received 22 October 2017; published 29 January 2018)

In this paper we investigate the complex dynamics originated by a cross-diffusion-induced subharmonic destabilization of the fundamental subcritical Turing mode in a predator-prey reaction-diffusion system. The model we consider consists of a two-species Lotka-Volterra system with linear diffusion and a nonlinear cross-diffusion term in the predator equation. The taxis term in the search strategy of the predator is responsible for the onset of complex dynamics. In fact, our model does not exhibit any Hopf or wave instability, and on the basis of the linear analysis one should only expect stationary patterns; nevertheless, the presence of the nonlinear cross-diffusion term is able to induce a secondary instability: due to a subharmonic spatial resonance, the stationary primary branch bifurcates to an out-of-phase oscillating solution. Noticeably, the strong resonance between the harmonic and the subharmonic is able to generate the oscillating pattern albeit the subharmonic is below criticality. We show that, as the control parameter is varied, the oscillating solution (sub$T$ mode) can undergo a sequence of secondary instabilities, generating a transition toward chaotic dynamics. Finally, we investigate the emergence of sub$T$-mode solutions on two-dimensional domains: when the fundamental mode describes a square pattern, subharmonic resonance originates oscillating square patterns. In the case of subcritical Turing hexagon solutions, the internal interactions with a subharmonic mode are able to generate the so-called "twinkling-eyes" pattern.

DOI: 10.1103/PhysRevE.97.012220

I. INTRODUCTION

In this paper we want to investigate the complex spatiotemporal dynamics emerging from a subharmonic destabilization of a primary subcritical Turing pattern in a simple predator-prey reaction-diffusion system.

Spatiotemporal oscillatory and irregular behavior in reaction-diffusion systems are generally ascribed to the interaction between Turing and Hopf instabilities, which can occur either through a codimension-two Turing-Hopf bifurcation [1–7] or due to different competing bifurcations of multiple steady states [8,9]. In particular, the observed dynamics in the proximity of a codimension-two Turing-Hopf bifurcation point can be classified in two different groups: the first includes the dynamics resulting from the interplay between a Turing mode and a Hopf mode. The resulting structures are typified by bistability, localized patterns, and mixed modes, i.e., oscillating structures characterized by the presence of one wave number k_c and one frequency ω_c, with all peaks oscillating synchronously (in-phase oscillations). The second group consists of dynamical behaviors originated by subharmonic instabilities of the Turing and the Hopf modes. A subharmonic Turing mixed mode (sub$T$ mixed mode), for example, results when the root of the characteristic equation corresponding to the subharmonic of the Turing mode, with wave number $k_c/2$, crosses the imaginary axis with nonzero imaginary part ($\omega[k_c/2] \neq 0$). In this case a resonance between the Turing mode with wave-number-frequency couple $(k_c,0)$ and its subharmonic mode $(k_c/2,\omega[k_c/2])$ originates an oscillating pattern with two wave numbers oscillating in time with one frequency [8]: the subharmonic then oscillates out of -phase with the fundamental mode.

Subharmonic T modes have been found in the presence of bulk oscillations, originated either from a Hopf instability [1,5,10], or from spatially uniform external periodic forcing [4,11], or in coupled layers of oscillators [12–15].

In this paper we propose a simple mechanism able to generate subharmonic T modes in absence of Hopf or wave bifurcations: keeping a simple form of the Lotka-Volterra type for the kinetic term, we assume that the movements of the individuals of the predator species are determined by classical random diffusion and by a taxis term down the gradient of prey. This model had previously appeared in [16], and we postpone to Sec. II a discussion on the physical motivations of the model.

In particular, we show that in a monostable regime where the linear stability analysis predicts the existence of a stationary pattern, temporal oscillations and chaos emerge. The occurrence of a wide variety of spatiotemporal patterns including regular and irregular oscillations is not new in spatially distributed predator-prey systems but it is usually induced by the presence of kinetic terms with a high degree of nonlinearity [17–22]. Differently from all these approaches, we adopt a particularly simple form for the reaction term which does not support any oscillatory instability, and prove the nonlinear cross-diffusion term to be the effective promoting factor for

[*]gaetana.gambino@unipa.it
[†]mariacarmela.lombardo@unipa.it
[‡]Corresponding author: marcomarialuigi.sammartino@unipa.it

the occurrence of a resonant mechanism resulting in regular and aperiodic oscillations.

We start our analysis on one-dimensional (1D) spatial domains where the cross-diffusion term allows, in the presence of a subcritical Turing band, for the onset of an internal subharmonic instability of the critical mode that gives rise to a stable out-of-phase oscillating mixed state. Furthermore, as the control parameter is varied, we show that the sub$T$ solutions undergo a phase instability, which produces successive bifurcations leading to quasiperiodicity, transient temporal chaos, and temporal chaos [23,24]. A similar transition has been recently reported in the Barrio-Varea-Aragon-Maini model [25–27], where a detailed numerical investigation had identified in the presence of competing cubic terms in the kinetics the main ingredient for the observed Ruelle-Takens-Newhouse route to chaos.

We stress the fact that in our model the spatiotemporal patterns are only due to the presence of the nonlinear cross-diffusion term. The crucial role played by cross-diffusion terms in establishing the emergence of an oscillatory Turing pattern in absence of any Hopf instability was pointed out also in [28], where linear cross diffusion and Michaelis-Menten functional response were considered. It is also noteworthy that recently out-of-phase oscillating Turing patterns were reported in a bistable reaction-diffusion system describing enzymatic reactions in a parameter region where no Hopf bifurcation is expected [29].

On one dimensional spatial domains, increasing the size of the domain, we shall also see the emergence of spatiotemporal chaos.

On two-dimensional (2D) domains we show resonant subharmonic interactions of stationary square patterns and subcritical Turing hexagons. In this latter case, the interplay between the static and the oscillatory subharmonic instability originates the "twinkling-eyes" pattern [30], first found theoretically as a resonant interaction between a Turing and a wave instability [31,32].

The plan of the paper is the following: In Sec. II we introduce the model and briefly recall the main outcomes of the linear stability analysis close to the homogeneous equilibrium. In Sec. III we discuss the bifurcation analysis leading to the formation of oscillatory patterns and the transition to spatiotemporal chaotic dynamics. In Sec. IV we extend our investigation to the case when the spatial domain is two-dimensional: we perform a weakly nonlinear analysis close to the bifurcation threshold, derive the normal forms for the Turing patterns, and elucidate the occurrence of oscillatory dynamics, twinkling-eye patterns and transition to irregular behavior.

II. MODEL AND LINEAR ANALYSIS

The proposed system describes a predator-prey model such that the predator movement is directed toward areas of low prey density. Therefore the presence of the prey affects movements of the predator in such a way that the latter avoids the zones with high prey density to enhance its hunting success. In fact, there is evidence that, for many species, living in aggregation can be an effective predator-avoidance tactic, so that the hunting success of predators generally decreases with prey group size.

The assumption of "negative aggregation" [33] for the movement of the predators chasing the preys, gives rise in our model to a nonlinear cross-diffusion term. Density-dependent self- and cross-diffusion terms were first introduced by Shigesada *et al.* to model spatial segregation of competing species [34]. Since then, strongly coupled reaction-diffusion systems with linear and nonlinear self- and cross-diffusion terms have been extensively applied to many different physical, chemical, and biological systems and their pattern-forming properties thoroughly investigated [35–42].

On the other hand, predator-prey systems have been observed to exhibit complex spatiotemporal dynamics, which includes, other than stationary patterns, regular and irregular oscillations, propagating fronts, spiral waves, pulses, patchiness, and chaotic oscillations. In order to elucidate the mechanisms underlying this richness of possible dynamics, different modeling approaches have been proposed: spatial variations of the environment [43–45], Allee effect [46–48], and predator invasion [49,50], just to name a few.

The model we consider here [16], in its nondimensional form reads

$$\begin{aligned} \partial_t u &= \Gamma u(r-\gamma u - v) + \nabla^2 u, \\ \partial_t v &= \Gamma v(-1+u) + d_{21}\nabla(v\nabla u) + d_2\nabla^2 v, \end{aligned} \tag{1}$$

where $u(x,t)$ and $v(x,t)$ indicate the population densities of preys and predators, respectively, and $x \in \Omega$, where Ω is a bounded fixed domain. In this and in the following section we shall assume $\Omega \subset \mathbb{R}$. The reaction term of model (1) is of the Lotka-Volterra predator-prey type with a logistic growth for the preys, where the nonnegative coefficients r and γ denote the growth rate and the inverse carrying capacity of u, respectively, and Γ is a measure of the relative strength of the kinetic term.

In the second equation the nonlinear diffusion term $d_{21}\nabla(v\nabla u)$ describes the tendency of the predator species v to keep away from high-density areas of the prey, preferring low-density areas of preys for hunting. The positive coefficients d_2 and d_{21} are the diffusion rate of the predator and the cross-diffusion rate, respectively. We shall impose homogeneous Neumann boundary conditions, as we assume that no external input is imposed from the outside.

The only spatially homogeneous stationary solution of (1) is $(u_0,v_0) = (1, r-\gamma)$ which has biological relevance only if $r-\gamma > 0$, a condition that will be supposed to hold throughout the rest of the paper.

Linearizing the system around (u_0,v_0) one gets

$$\mathbf{w}_t = \Gamma \mathrm{J}\mathbf{w} + D\nabla^2\mathbf{w}, \quad \mathbf{w} = \begin{pmatrix} u-u_0 \\ v-v_0 \end{pmatrix}, \tag{2}$$

where

$$J = \begin{pmatrix} -\gamma & -1 \\ r-\gamma & 0 \end{pmatrix}, \quad D = \begin{pmatrix} 1 & 0 \\ d_{21}v_0 & d_2 \end{pmatrix}. \tag{3}$$

The equilibrium point is linearly stable, being an attractive node for $\gamma < r < \gamma + \gamma^2/4$ or an attractive spiral for $r > \gamma + \gamma^2/4$. Since $\mathrm{tr}(J) = -\gamma$ is always negative, this system does not support any Hopf bifurcation, which would require $\mathrm{tr}(J) = 0$.

To investigate the conditions for diffusion-driven instability, we construct the matrix $A(k) = \Gamma J - k^2 D$. If there is an

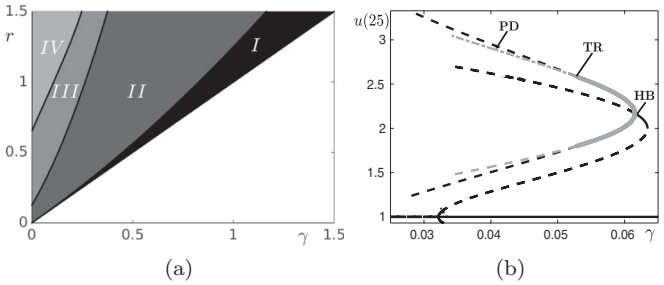

FIG. 1. (a) The Turing instability region $r > \gamma$ is shown for the parameter set $\Gamma = 5$, $d_2 = 1$: regions I (nodes) and II (spirals) correspond to the supercritical Turing bifurcation; regions III (spirals) and IV correspond to the subcritical case. The numerically computed boundary between regions III and IV corresponds to the locus of the subharmonic bifurcation (see Sec. III). (b) Numerically computed bifurcation diagram of the species u at the central spatial point as γ is varied: stable and unstable stationary branches are represented by solid and dashed black lines, respectively; stable and unstable oscillatory solutions are represented by solid and dashed gray lines, respectively.

eigenvalue λ of $A(k)$ with positive real part, for some $k \neq 0$, then the spatially homogeneous equilibrium is destabilized by a periodic perturbation of wavelength $2\pi/k$, exponentially growing with time.

We observe that $\mathrm{tr}[A(k)] = -\Gamma\gamma - k^2(d_2 + 1) < 0$, therefore the system does not support oscillations with $k \neq 0$ either. Therefore, according to the linear stability analysis, oscillations are prohibited.

Choosing d_{21} as bifurcation parameter, in [16] a stationary (Turing) bifurcation was found to occur at the following critical values:

$$d_{21}^c = \frac{\gamma d_2 + 2\sqrt{\det(J)\det(D)}}{\det(J)}, \tag{4}$$

$$k_c^2 = \Gamma\sqrt{\frac{\det(J)}{d_2}}. \tag{5}$$

In Fig. 1(a), in the parameter space (γ, r) we report the zone $r > \gamma$ where Turing instability can develop. This region is further divided into four distinct domains: in region I, the stable equilibrium point is a node; in regions II, III, and IV it is a spiral. The numerically computed boundary between regions II and III separates the supercritical Turing instability, i.e., region II, from the subcritical case, regions III and IV. The boundary between regions II and III is computed imposing the Landau coefficient of the amplitude equation to be zero (see next section for more details). In region IV, subharmonic instability leads to oscillations (see next section).

In Figs. 2(a)–2(d) the real and imaginary parts of the eigenvalues are plotted as a function of k in the four different regions of the (γ, r)-parameter space: in regions I and II, one has a supercritical Turing band (positive real part of the maximum eigenvalue and zero imaginary part in correspondence to a band of positive wave numbers), while in regions III and IV the Turing band is subcritical. In all four regions, the $k = 0$ mode has negative Reλ, corresponding to the absence of uniform oscillatory instabilities.

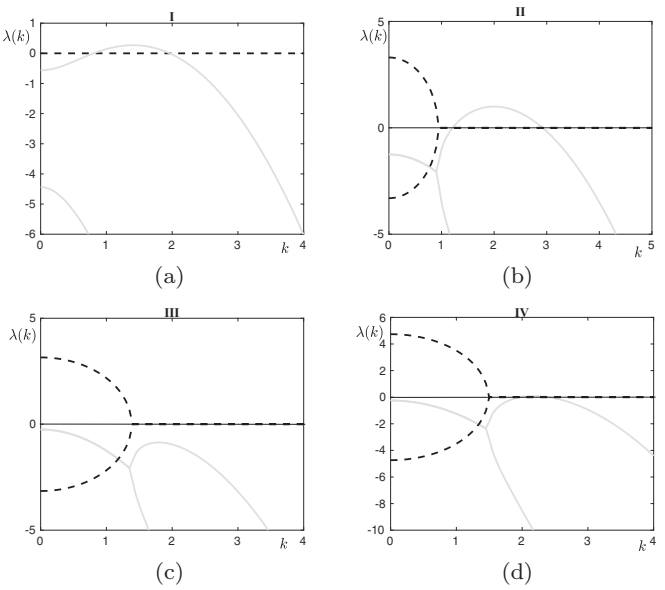

FIG. 2. Dispersion relation for the regions I–IV. The real and the imaginary part of the eigenvalues are plotted by gray solid lines and by black dashed lines, respectively: All the curves have $\Gamma = 5$, $d_2 = 1$. (a) Region I: $r = 1.1$, $\gamma = 1$,$d_{21} = 19$. (b) Region II: $r = 1$, $\gamma = 0.5$, $d_{21} = 5$. (c) Region III: $r = 0.5$, $\gamma = 0.1$, $d_{21} = 2.6$. (d) Region IV: $r = 1$, $\gamma = 0.1$, $d_{21} = 2.28$.

In Fig. 3 the dependence of the maximum of Re(λ) on the cross-diffusion coefficient d_{21} is reported: one can observe that, moving from region I toward region IV, the critical value of the bifurcation parameter d_{21}^c decreases, while the maximum value of the real part of the eigenvalue becomes larger.

III. SUBHARMONIC INSTABILITY AND BIFURCATION ANALYSIS

A. Subharmonic resonance

In [16] a detailed weakly nonlinear analysis investigating the resulting patterns in the parameter regions corresponding to both the supercritical and the subcritical Turing bifurcation was performed. Here we shall focus on the region lying on the left of the boundary between regions II and III of the (r, γ)-parameter space shown in Fig. 1(a) where, according to the weakly nonlinear analysis, one should expect a subcritical

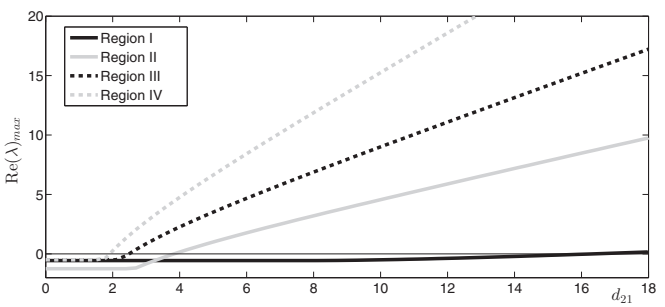

FIG. 3. Depencence of maximum of Re(λ) at $k = k_c$ on the cross-diffusion coefficient in the regions I–IV. The parameter values are chosen as in Figs. 2(a)–2(d), respectively.

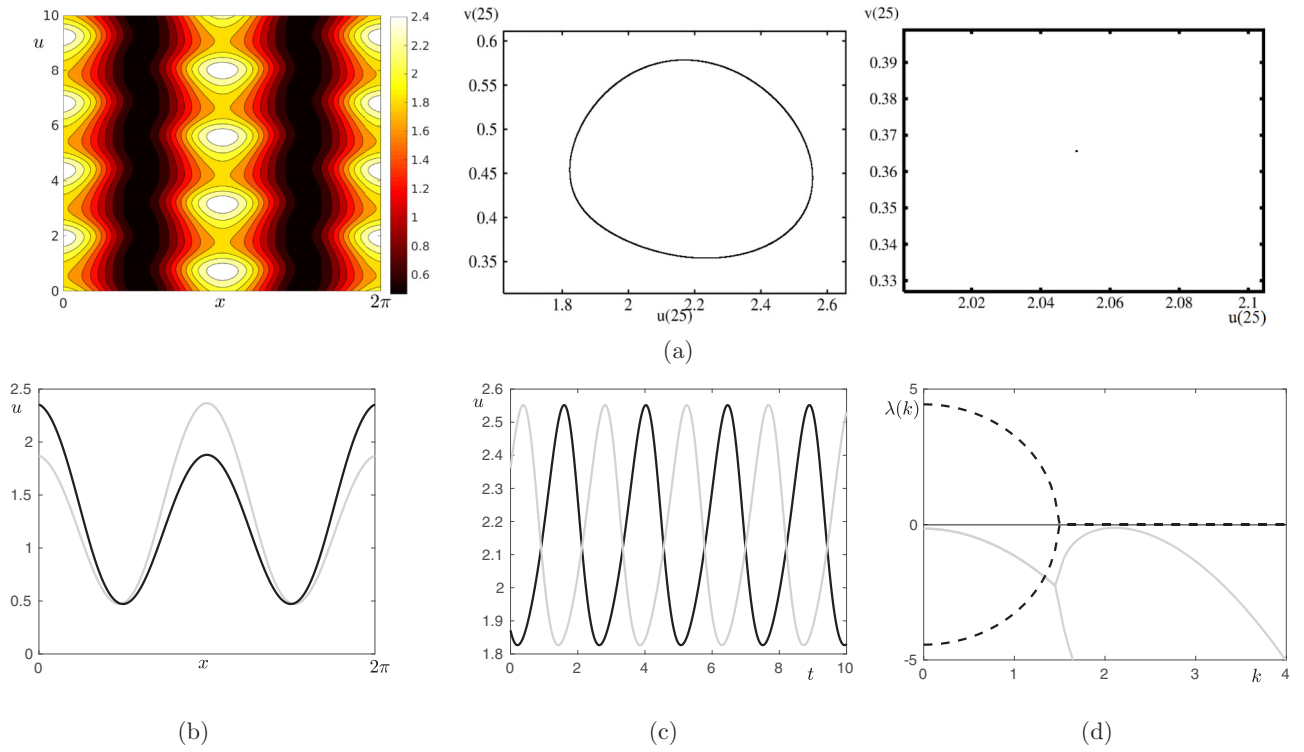

FIG. 4. Out-of-phase oscillatory Turing patterns: (a) The parameter values are chosen as in Fig. 1(b) and $\gamma \simeq 0.053\,83$. Left: space-time evolution of u with $x \in [0,2\pi]$ on the horizontal axis and time increasing from *bottom* to *top*. Center: phase portrait of $v(25)$ vs $u(25)$. Right: Poincaré section at $u(27) = 2$. (b) Black and gray curves are two antiphase patterns separated in time by $T/2 \simeq 1.21$. (c) Black and gray curves are two-phase oscillations at locations separated in space by $\lambda_c = \pi$. (d) Dispersion relation at the Hopf bifurcation: $\gamma = 0.0615$. The real and the imaginary parts of the eigenvalues are plotted by gray solid lines and by black dashed lines, respectively.

stationary Turing pattern. It is worth recalling that the kinetic term of (1) does not exhibit any Hopf bifurcation so that, in the whole region, the equilibrium point is a stable spiral in absence of diffusion. On the basis of the linear stability analysis one should therefore expect a pure Turing instability, giving rise to a stationary pattern. As pointed out in [16], this is not the case if the system parameters are chosen well inside the subcritical region, i.e., in region IV of Fig. 1(a). Fixing the parameters d_{21}, d_2 and r so that a subcritical Turing pattern is obtained and decreasing the parameter γ, the stationary pattern is destabilized by disturbances twice its wavelength so that time oscillations of the periodic structure are observed. Such oscillations are to be ascribed to the resonance between the fundamental subcritical Turing mode and its $1/2$ subharmonic: with decreasing γ, in fact, there exists a critical value of the amplitude of the critical mode beyond which the instability triggers an efficient transfer of energy to the $1/2$ mode, which oscillates with frequency $\omega[k_c/2]$, out of phase with the fundamental.

We shall therefore investigate the system dynamics using γ as a control parameter. The system is numerically solved with a finite difference scheme based on the method of the lines, where the equations are first discretized with respect to the spatial variable. The resulting semidiscrete ordinary differential equation system is then integrated in time. A standard second-order centered difference scheme is adopted to approximate the Laplacian term while the nonlinear diffusion term is approximated by a second-order finite difference algorithm. For the time integration we used the CVODE stiff integrator included in the XPPAUT computational software package. We set error tolerances of 10^{-10}, and used a time step $\Delta t = 10^{-3}$ and a spatial mesh size with $N = 50$ nodes on the interval $[0,2\pi]$, where Neumann boundary conditions are imposed.

We choose the following parameter values: $r = 0.85$, $\Gamma = 5$, $d_2 = 1$, $d_{21} = 2.269$, in a way that, on the basis of the weakly nonlinear analysis, the stationary Turing pattern is expected to bifurcate subcritically from the homogeneous steady state at $\gamma \simeq 0.032\,17$. The linear analysis and the imposed boundary conditions predict that the most rapidly growing mode is $k_c = 2$. In fact, for $\gamma > 0.032\,17$, a stable spatially periodic stationary pattern is formed, which displays the expected wavelength. To illustrate the outcomes of the simulations and investigate the system dynamics far from the primary bifurcation, in Fig. 1(b) we report the numerical bifurcation diagram, obtained with the software AUTO.

In Fig. 1(b) one can see the subcritical Turing branch bifurcating from the homogeneous equilibrium. At $\gamma \simeq 0.061\,53$, the Turing branch loses stability due to a subharmonic resonance: the resonant interaction between the fundamental mode and its subharmonic, determines the birth of oscillating-in-time, periodic-in-space structures. A representative numerical simulation, for $\gamma = 0.053\,83$, is reported in Fig. 4(a): on the left the space-time map of the resulting oscillatory Turing pattern is shown, which corresponds to a limit cycle in the phase space of the central points (reported in the middle column). The

Poincaré section at $u(27) = 2$ is displayed in the right column, showing a fixed-point steady state. We notice that, at each spatial location, the system oscillates with one frequency but, because of the presence of the two wave numbers k_c and $k_c/2$, the minima of the pattern are shifted one wavelength every half period of oscillation (a subharmonic mixed mode or sub$T$ mode). This behavior can also be discerned from Fig. 4(b), where the u profiles obtained at two different times separated by $T/2$ are depicted. In Fig. 4(c) we report the antiphase oscillations at two neighboring Turing extrema (separated by $\lambda_c = \pi$). In Fig. 4(d) we report the dispersion relation at the onset of the sub$T$-mode: it shows that both the fundamental ($k_c = 2$) and its 1/2-subharmonic are subcritical, so that in the proposed model out-of-phase oscillations can arise at negative Re(λ). The Fourier spectrum of the spatial profile of the two species (not shown here) displays two significantly nonzero amplitudes corresponding to the excited modes oscillating in time: the critical mode k_c and the mode $k_c/2$. The numerically computed value of the period of oscillations fits quite well with the expected value $T = 2\pi/\omega(k_c/2)$, where $\omega(k_c/2)$ is the imaginary part of the eigenvalue at $k = k_c/2$.

We have numerically computed the bifurcation diagram corresponding to the onset of the sub$T$ mode, for different values of the parameter r, therefore obtaining, in the (γ,r)-Turing space, the locus of subharmonic instability threshold. The corresponding curve is plotted in Fig. 1(a), separating region III, where a stationary Turing pattern is observed, from region IV, where spatiotemporal oscillations emerge.

B. Temporal and spatiotemporal chaos

In this section we explore the possibility of chaotic temporal and spatiotemporal dynamics: in fact, as the parameter γ is decreased while maintaining all the other parameters fixed as in Sec. III A, one observes the occurrence of successive bifurcations which eventually lead to temporal chaotic solutions. At $\gamma \simeq 0.052\,73$ the oscillatory sub$T$ mode undergoes a torus bifurcation, which introduces a second frequency in the temporal dynamics of system (1). The corresponding numerical simulation for $\gamma = 0.052\,02$ is reported in Fig. 5(a), showing also the expected limit cycle in the Poincaré section. In Fig. 6 we report the corresponding power spectrum, where sharp peaks are identified, each of which can be matched to a linear combination of the two frequencies characteristic of the motion on a 2-torus.

As γ is further decreased, a period-doubling bifurcation occurs at the value $\gamma = 0.039\,38$, after which the system exhibits quasiperiodic behavior [see Fig. 5(b)]. Further decrease of the parameter γ induces the occurrence of temporal chaotic dynamics. Indeed the chaotic behavior is not asymptotically stable: after some time, in fact, it collapses, evolving toward a periodically oscillating solution. This scenario is exemplified in Figs. 5(c) and 5(d), where we report the system behavior at $\gamma = 0.029\,75$: the dynamics is initially characterized by the presence of temporally aperiodic oscillations, which are shown in the left panel of Fig. 5(c) and can also be deduced from the complex nested pattern of the phase-space plot [middle panel of Fig. 5(c)] and from the scattered points displayed in the Poincaré section [right panel of Fig. 5(c)]. The temporal chaos persists up to approximately 60 time units, after which the system settles in a stable periodically oscillating pattern. The dynamics from $t \simeq 500$ is shown in Fig. 5(d): both the phase-space and the Poincaré section indicate the presence of a periodic-in-time orbit.

As the control parameter is further decreased, the oscillating subharmonic pattern becomes, in fact, phase unstable, giving rise to a transition to temporal broadband turbulence [see Fig. 5(e) and the inset of Fig. 6]. This transition has also been observed in other systems presenting subharmonic instabilities [1,23].

The transient nature of chaotic dynamics described above and shown in Figs. 5(c) and 5(d) is not new and has been found in several reaction-diffusion systems [51–57]. Since it is known that the chaos lifetime increases exponentially with system size [58], in the rest of this section we shall investigate the system size dependence of the chaotic dynamics by considering different system sizes.

We choose the following parameter values: $r = 1.5$, $\gamma = 0.22$, $d_2 = 1$, $d_{21} = 2.269$, which on the basis of the weakly nonlinear analysis, prescribe the presence of a subcritical Turing pattern. We then consider different domain sizes by varying the parameter Γ, whose square root is proportional to the linear size of the domain.

For small system sizes (small values of Γ), the oscillating pattern induced by the subharmonic instability is stable. This is shown in Fig. 7(a), where the space-time plot for $\Gamma = 3.535$ is displayed, which corresponds to a system size equal to four times half of the spatial wavelength λ of the pattern. In the case of small domain sizes, stable oscillatory patterns are also found when the value of Γ is such that the domain size is not an integer multiple of $\lambda/2$. Increasing the value of Γ corresponds to the occasional missing of a beat or to periodic movements of the maxima of the pattern, as is shown in Fig. 7(b), where $\Gamma = 7.955$ has been selected, which corresponds to a domain size equal to six times $\lambda/2$. A critical value of $\Gamma \simeq 14.14$ has been identified, which corresponds to a domain size approximately equal to eight times $\lambda/2$, above which the system presents spatiotemporal chaotic behavior. This is displayed in Figs. 7(c) and 7(d), obtained for $\Gamma = 43.31$ (corresponding to a domain size equal to 14 times $\lambda/2$) and $\Gamma = 83.388$ (corresponding to a domain size equal to 20 times $\lambda/2$), respectively. The space-time plot of the corresponding dynamics shows the presence of merging and splitting of maxima, and of phase slips, all elements that characterize spatiotemporal chaos [54].

IV. 2D PATTERNS

To investigate the formation and stability of coherent solutions to the system (1) on the two-dimensional rectangular domain $\Omega = [0, L_x] \times [0, L_y]$ we perform a weakly nonlinear (WNL) analysis so to derive a reduced description of the resulting patterns in terms of their amplitude [59,60]. Restricting our analysis to the cases where the homogeneous steady state bifurcates at a single or a double eigenvalue, we are able to characterize the type of supported patterns as follows:

(i) rolls and square-rhombic patterns when the bifurcation occurs via a single eigenvalue;

(ii) mixed-mode patterns when the bifurcation occurs via a double eigenvalue and the no-resonance condition holds;

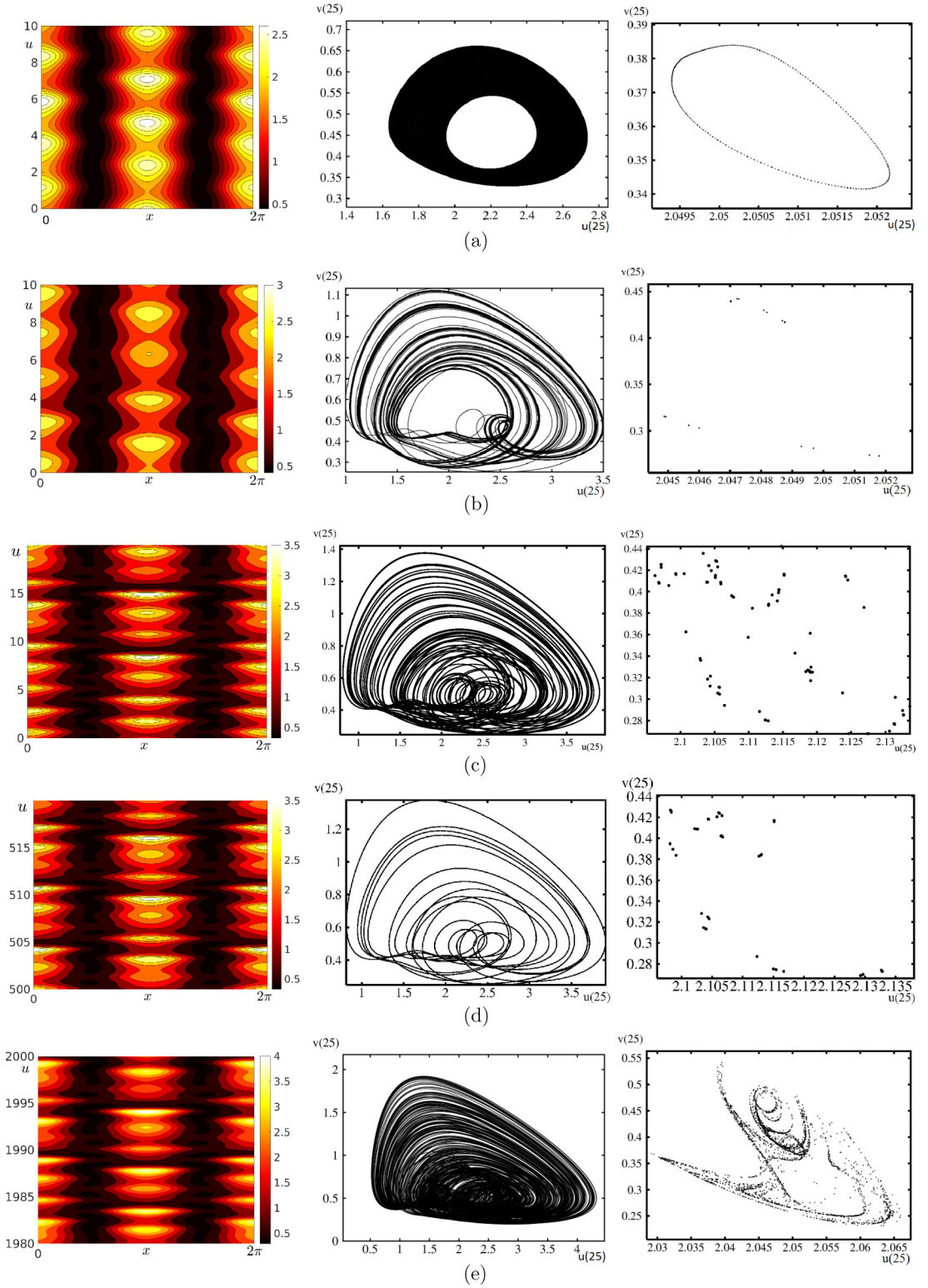

FIG. 5. Dynamical behaviors at different values of γ: transition to temporal chaos. Left: space-time evolution of u with $x \in [0,2\pi]$ on the horizontal axis and time increasing from *bottom* to *top*. Center: phase portrait of $v(25)$ vs $u(25)$. Right: Poincaré sections at $u(27) = 2$. (a) $\gamma = 0.052\,02$: dynamics on a torus which corresponds to a limit cycle in the Poincaré map; (b) $\gamma = 0.035\,05$: quasiperiodic motion; (c) $\gamma = 0.029\,75$, up to $t = 20$: transient temporal chaos; (d) $\gamma = 0.029\,75$ from $t = 500$: the system has settled in a stable oscillatory motion; (e) $\gamma = 0.027\,92$: temporal chaos.

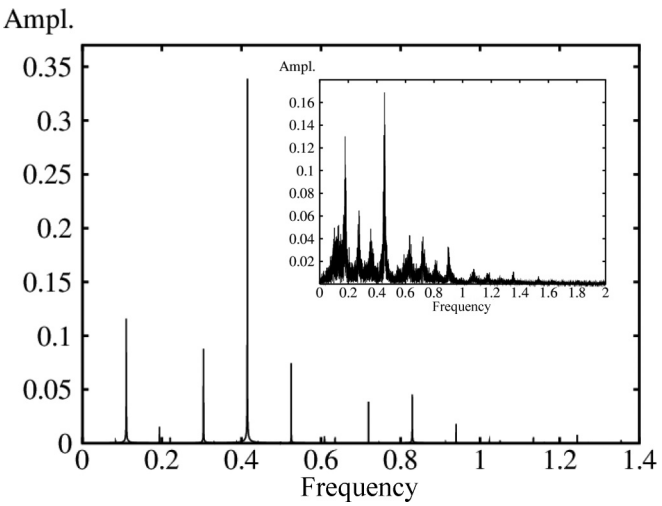

FIG. 6. Fourier power spectrum for $\gamma = 0.051\,16$ at $t = 300$ (after 300 000 iterations), displaying the typical peaks of a torus dynamics. Inset: Broadband continuous power spectrum obtained for $\gamma = 0.028\,19$, characteristic of chaotic behavior.

(iii) hexagonal patterns when the bifurcation occurs via a double eigenvalue and the resonance condition holds.

Here we skip the technical details of the analysis in all the above considered cases (see [59] for a full description), and simply report the resulting normal forms.

In case (i), there exists a unique couple of integers (m,n) such that

$$k_c^2 \equiv \phi^2 + \psi^2 \quad \text{where} \quad \phi \equiv \frac{m\pi}{L_x}, \quad \psi \equiv \frac{n\pi}{L_y}.$$

The WNL multiple scale analysis leads to finding the evolution equation for the amplitude of the pattern, which is the following Stuart-Landau equation:

$$\frac{dA}{dT_2} = \sigma A - LA^3. \tag{6}$$

When the model parameters are such that bifurcation is supercritical (i.e., $L > 0$), the emerging solution of the reaction-diffusion system (1) close to the onset is given by

$$\mathbf{w} = \varepsilon \boldsymbol{\rho} A_\infty \cos(\phi x)\cos(\psi y) + O(\varepsilon^2), \tag{7}$$

where ε measures the square root of the distance of the control parameter from the bifurcation value, A_∞ is the stable stationary state of the Stuart-Landau equation (6), and $\boldsymbol{\rho} \in \mathrm{Ker}(\Gamma J - k_c^2 D)$. The solutions in (7) are rhombic spatial patterns, whose special cases are the rolls (when either ϕ or ψ is zero) or the squares (when $\phi = \psi$).

In case (ii), there exist two couples of integers (m_i,n_i), $i = 1,2$ such that

$$k_c^2 \equiv \phi_i^2 + \psi_i^2 \quad \text{where} \quad \phi_i \equiv \frac{m_i\pi}{L_x}, \quad \psi_i \equiv \frac{n_i\pi}{L_y}, \tag{8}$$

and the following no-resonance condition holds:

$$\begin{aligned} &\phi_k + \phi_j \neq \phi_j \quad \text{or} \quad \psi_k - \psi_j \neq \psi_j \\ &\text{and} \\ &\phi_k - \phi_j \neq \phi_j \quad \text{or} \quad \psi_k + \psi_j \neq \psi_j \end{aligned} \tag{9}$$

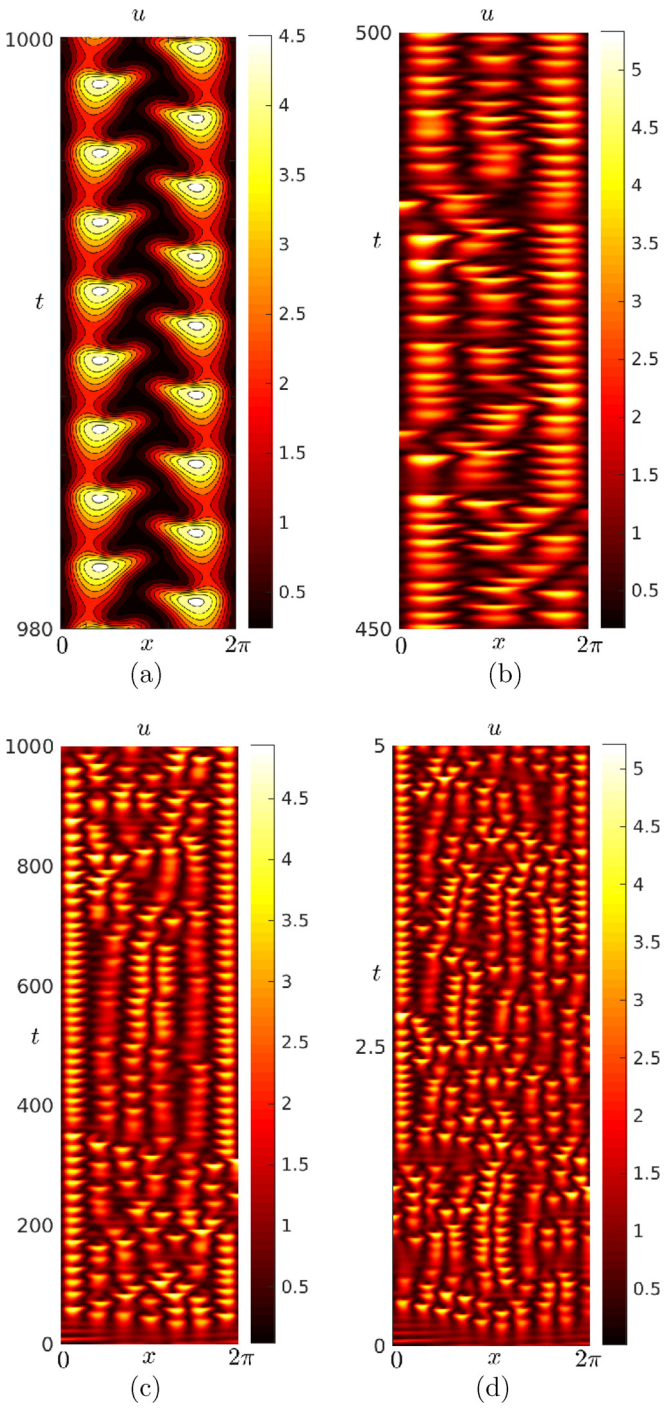

FIG. 7. Space-time plots for different system sizes. All the plots have $r = 1.5$, $\gamma = 0.22$, $d_2 = 1$, $d_{21} = 2.269$, and different values of Γ. (a) $\Gamma = 3.535$, corresponding to a ratio between the domain size and $\lambda/2$ of 4: the out-of-phase oscillating pattern is stable. (b) $\Gamma = 7.955$, corresponding to a ratio between the domain size and $\lambda/2$ of 6: the oscillatory structure is destabilized by occasional irregularities. (c) $\Gamma = 43.31$, corresponding to a ratio between the domain size and $\lambda/2$ of 14: the pattern displays merging, splitting, and phase slips phenomena, typical of spatiotemporal chaos. (d) $\Gamma = 83.388$, corresponding to a ratio between the domain size and $\lambda/2$ of 20: fully chaotic spatiotemporal dynamics.

with $k,j = 1,2$ and $k \neq j$. Performing the WNL analysis, one finds that the two different amplitudes A_1 and A_2 which characterize the resulting pattern are governed by the following system of two coupled Landau equations:

$$\frac{dA_1}{dT} = \sigma A_1 - L_1 A_1^3 + R_1 A_1 A_2^2, \tag{10a}$$

$$\frac{dA_2}{dT} = \sigma A_2 - L_2 A_2^3 + R_2 A_1^2 A_2. \tag{10b}$$

If the system (10) admits at least one stable equilibrium $(A_{1\infty}, A_{2\infty})$, the emerging asymptotic solution of the reaction-diffusion system (1) is correctly approximated by

$$\mathbf{w} = \varepsilon \boldsymbol{\rho} \sum_{i=1}^{2} A_{i\infty} \cos(\phi_i x) \cos(\psi_i y) + O(\varepsilon^2). \tag{11}$$

The solutions in (11) describe the so-called mixed-mode patterns, complex structures arising due to the interaction of different modes ϕ_i, ψ_i. They reduce to the rhombic spatial patterns found in case (i) when either one between $A_{1\infty}$ and $A_{2\infty}$ is zero.

Finally, in case (iii), there exist two couples of integers such that (8) is satisfied and the following resonance condition holds:

$$\begin{aligned} &\phi_k + \phi_j = \phi_j \quad \text{and} \quad \psi_k - \psi_j = \psi_j \\ &\text{or} \\ &\phi_k - \phi_j = \phi_j \quad \text{and} \quad \psi_k + \psi_j = \psi_j \end{aligned} \tag{12}$$

with $k,j = 1,2$ and $k \neq j$. Through the WNL asymptotic analysis, we recover at $O(\varepsilon^2)$ a dynamical system governing the evolution of the pattern amplitudes which does not admit stable equilibria in any parameter regime: this returns a subcritical transition. Pushing the analysis at $O(\varepsilon^3)$, we find the following system for the amplitudes A_1 and A_2:

$$\begin{aligned} \frac{dA_1}{dT} &= \sigma_1 A_1 - L_1 A_1 A_2 + R_1 A_1 A_2^2 + S_1 A_1^3, \\ \frac{dA_2}{dT} &= \sigma_2 A_2 - L_2 A_1^2 + R_2 A_1^2 A_2 + S_2 A_2^3. \end{aligned} \tag{13}$$

Assuming, without loss of generality, that the second condition in (12) holds with $i = 2$ and $j = 1$, and taking into account the relation in (8), it follows that $\phi_2 = 2\phi_1$, $\psi_2 = 0$, $\psi_1 = \sqrt{3}\phi_1$, $\phi_1 = k_c/2$, and $L_y = \sqrt{3}L_x$. If the system (13) admits at least one stable equilibrium, the emerging asymptotic solution of the reaction-diffusion system (1) at the leading order is approximated by

$$\begin{aligned} \mathbf{w} = \varepsilon \boldsymbol{\rho} [&A_{1\infty} \cos(\phi_1 x) \cos(\psi_1 y) \\ &+ A_{2\infty} \cos(\phi_2 x) \cos(\psi_2 y)] + O(\varepsilon^2), \end{aligned} \tag{14}$$

where $(A_{1\infty}, A_{2\infty})$ is a stable stationary state of the system (13). These solutions are hexagonal patterns or, in the case when $A_{1\infty} = 0$, rolls.

The outcomes of the WNL analysis constitute the starting point for the investigation of 2D oscillatory patterns. As in the case of the 1D domain, the oscillatory instability is generated by subharmonic resonances, involving secondary modes with lower wave number. We start considering the oscillatory instability of the subcritical hexagons. On the rectangular domain $L_x = 2\pi$ and $L_y = 2\sqrt{3}\pi$, we choose the parameter set such that the only unstable discrete mode is $k_c^2 = 36$, which corresponds to the two mode pairs (6,18) and (12,0) satisfying the condition (8). Numerical simulations, performed choosing as initial condition a small random perturbation of the equilibrium, show the evolution toward the stationary solution given in Fig. 8.

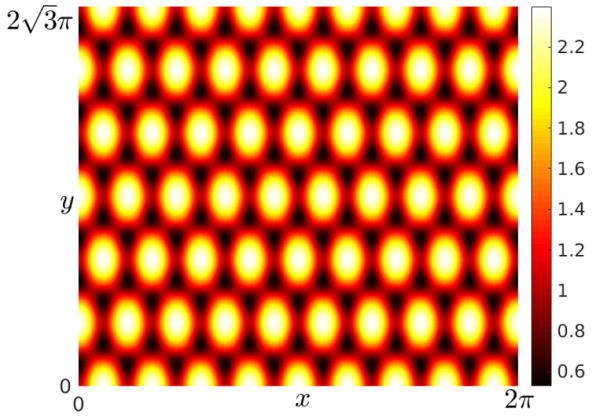

FIG. 8. The numerical solution of (1) asymptotically converges to the subcritical hexagonal pattern predicted by the WNL analysis. The parameters are chosen as $\Gamma = 45$, $r = 0.85$, $d_2 = 1$, $\gamma = 0.21$, $d_{21} = 2.8281$.

Its explicit form is captured by the following hexagonal pattern, predicted by the WNL analysis to be a stable subcritical solution of system (1):

$$\begin{aligned} \mathbf{w} = \varepsilon \boldsymbol{\rho} &\left[A_{1\infty} \cos(3x) \cos\left(\frac{9}{\sqrt{3}} y\right) + A_{2\infty} \cos(6x) \right] \\ &+ O(\varepsilon^2), \end{aligned} \tag{15}$$

where $(A_{1\infty}, A_{2\infty})$ is a stable equilibrium of the system (13).

Assuming now as initial condition the stationary pattern depicted in Fig. 8 and decreasing the value of γ to 0.2 (while maintaining all the other parameter values fixed), the numerical solution loses its stability and starts to oscillate in time. The snapshots of the twinkling-eye hexagons are shown in Fig. 9(a). The observed time oscillatory behavior is determined by the resonant interaction between the fundamental subcritical Turing mode, whose wave number is $k_c = 6$ and which gives rise to a stationary hexagonal lattice and its subharmonic mode. The sub$T$ has wave number $k_{\text{sub}} = k_c/\sqrt{(3)} \simeq 3.46$, and lies within the Hopf domain, i.e., $\text{Im}(\lambda) = \omega[k_c/\sqrt{(3)}] \neq 0$ [see Fig. 9(d)]. Although the sub$T$ has negative $\text{Re}(\lambda)$, the strong intrinsic coupling with the steady mode is able to induce a destabilization of the fundamental, which results in the development of a temporally oscillating subhexagonal lattice [11]. The hexagonal array of spots thus separates into three sets, each forming a hexagonal sublattice with wavelength $\sqrt{(3)}$ times the wavelength of the original lattice and shifted in phase by $2\pi/3$ from the other sublattices.

A further decrease in the value of γ induces secondary (Hopf) instabilities of the sub$T$ solution with the consequent birth of chaotic dynamics.

To show the emergence of oscillating square patterns, we consider the square domain $L_x = L_y = \pi$, and select

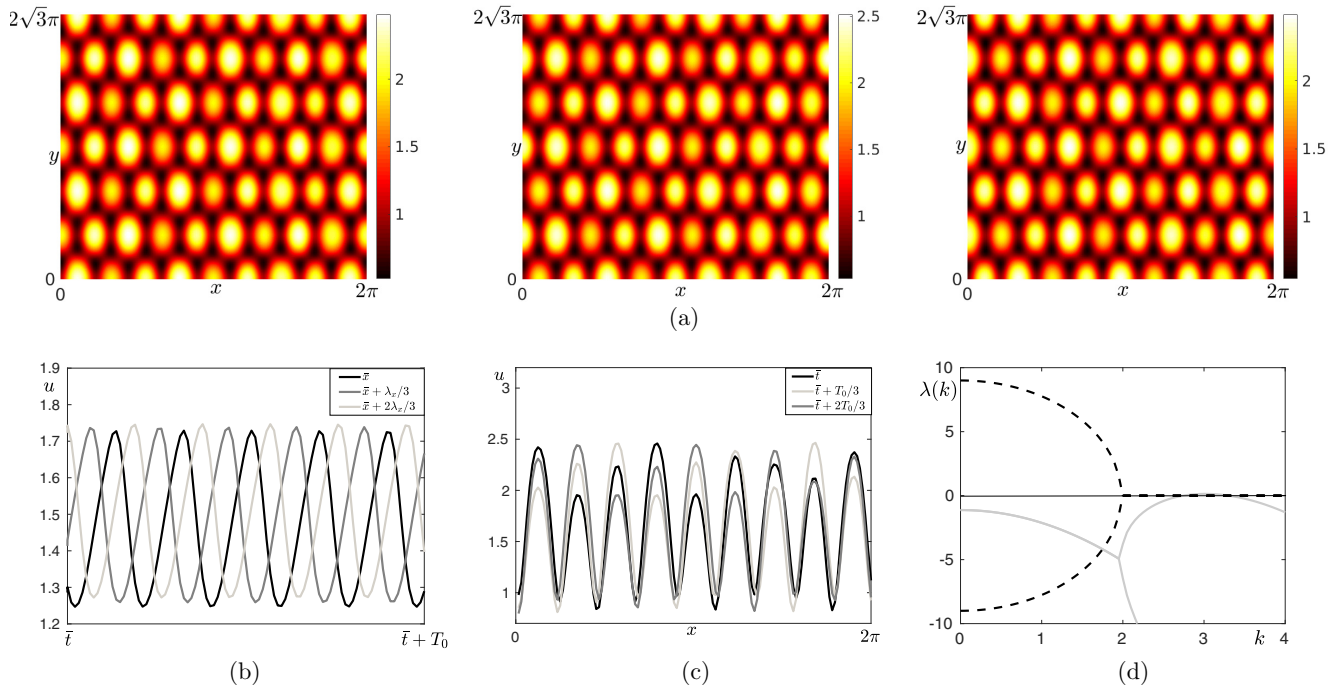

FIG. 9. Twinkling-eye hexagons: (a) All the parameter values are chosen as in Fig. 7 except γ, whose value is $\gamma = 0.2$. Snapshots of the hexagonal pattern taken at successive times. Left: at time t. Center: at time $t + T/3$. Right: at time $t + 2T/3$. (b) Black, light-gray, and gray curves are three sections of the pattern at $\bar{x} = 2.27$, $y = 3.8$ separated in time by $T/3 \simeq 0.12$ and showing out-of-phase oscillations. (c) Black, light-gray, and gray curves are three sections of the pattern at $y = 3.8$ at locations separated in space by $\lambda_c/3 = \pi/9$ showing three-phase oscillations. (d) Dispersion relation. The real and the imaginary parts of the eigenvalues are plotted by gray solid lines and by black dashed lines, respectively.

the following parameter values $\Gamma = 60.78$, $r = 0.85$, $d_2 = 1$, $\gamma = 0.2$, $d_{21} = 2.7884$. The most unstable discrete mode is given by $k_c^2 = 49$ and the condition (8) is satisfied by the two mode pairs (7,0) and (0,7). This parameter set returns a pattern belonging to case (ii) above; the WNL analysis then predicts that the system admits only the stable equilibria:

$$P^{(\pm,\pm)} \equiv \left(\pm \sqrt{\frac{\sigma(L_2 + \Omega_1)}{L_1 L_2 - \Omega_1 \Omega_2}}, \pm \sqrt{\frac{\sigma(L_1 + \Omega_2)}{L_1 L_2 - \Omega_1 \Omega_2}} \right), \quad (16)$$

so that the expected solution is the following square pattern:

$$\mathbf{w} = \varepsilon \boldsymbol{\rho} [A_{1\infty} \cos(7x) + A_{2\infty} \cos(7y)] + O(\varepsilon^2). \quad (17)$$

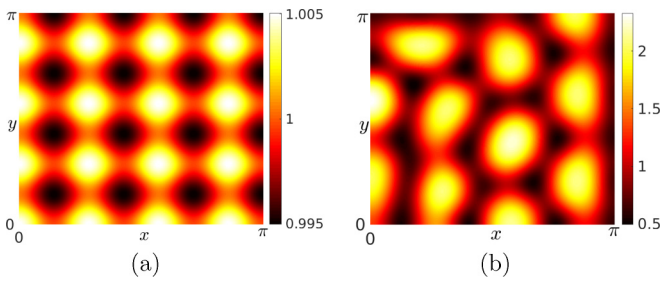

FIG. 10. (a) Snapshot of the stationary square pattern predicted by the WNL analysis. The system parameters are $\Gamma = 60.78$, $r = 0.85$, $d_2 = 1$, $d_{21} = 2.7884$, $\gamma = 0.2$. (b) Snapshot of the oscillatory pattern. The values of the parameters are as in (a), except $\gamma = 0.19$.

where $(A_{1\infty}, A_{2\infty})$ are the coordinates of the point $P^{(\pm,\pm)}$. Starting from the random periodic perturbation of the equilibrium, the numerical solution of the full system (1) in fact evolves to the square pattern whose amplitude is predicted by the WNL analysis and shown in Fig. 10(a). Assuming as initial condition the square pattern depicted in Fig. 10(a) and decreasing the value of γ to $\gamma = 0.19$ (while maintaining all the other parameter values fixed), the numerical solution loses its stability and jumps to a large amplitude subcritical solution, which, after a short transient, starts to oscillate in time. The snapshots of the spatiotemporal periodic pattern are shown in Fig. 10(b). In this case, therefore, the subcritical mode resonantly interacting with its subharmonic is not the critical mode predicted by the WNL analysis. In fact we conjecture that, with decreasing the value of γ, one induces a change in the expression of the coefficients of the normal form derived in case (ii), which now admits only unstable solutions. To predict the resulting critical mode (and its subharmonic) it would be then necessary to push the weakly nonlinear analysis to the fifth order and derive the explicit expression of the stable solutions to the quintic amplitude equations. This will be the subject of a subsequent paper.

V. CONCLUSIONS

In this paper we have investigated the complex dynamics supported by a novel predator-prey system with non-linear cross-diffusion term and quadratic Lotka-Volterra reaction kinetics. The nonlinear cross-diffusion term describes the

tendency of the predators to move in response to a spatially decreasing prey density to maximize prey suppression. The model was presented in [16], where it was shown how the introduction of the cross diffusion is critical to the formation of periodic structures, also in the presence of a trivializing kinetics. Moreover the detailed theoretical and numerical analysis performed in [16] on 1D domains allowed one to distinguish between supercritical and subcritical transitions to stationary periodic patterns. The occurrence in the numerical experiments of oscillating-in-time pattern solutions was also reported. In this paper we have deeply investigated the secondary instabilities induced by subharmonic resonance phenomena, leading to the spatiotemporal oscillating solutions and to the consequent transition to chaotic dynamics. With the aid of the numerical bifurcation diagram we have identified the region, in the parameter space, where the subcritical Turing branch undergoes a subharmonic destabilization, resulting in oscillations of the underlying periodic structure. This behavior is unexpected on the basis of the linear analysis and contradicts the belief that oscillations in a reaction-diffusion system can be obtained only in the presence of either a Hopf bifurcation in the local dynamics or a wave instability. In the proposed model the spatiotemporal periodic solutions are generated by a spatial resonance of the fundamental Turing mode with its subharmonic, whose corresponding growth rate has a nonzero imaginary part. Remarkably, the subharmonic mode is able to resonantly interact with the subcritical fundamental Turing mode, generating time oscillations, although its growth rate as predicted by the linear analysis, is negative. We have therefore detected the presence of a sequence of self-induced subharmonic instabilities, corresponding to the emergence of transient temporal chaos and fully chaotic-in-time solutions. Exploiting the dependence of the supported dynamics on the domain size, we have illustrated the transition from subharmonic-induced oscillations to spatiotemporal chaotic solutions as the domain size exceeds a critical value.

In the case of a two-dimensional spatial domain, we have derived the normal forms of the bifurcating stationary spatially periodic solutions, classifying the different resulting pattern as the parameters are varied in the Turing space. We have proved that the presence of the cross-diffusion term in a simple reaction-diffusion system is responsible for the formation of the twinkling-eye hexagons and other oscillating Turing patterns.

These results emphasize the need of further investigation of simple systems to better understand the mechanisms underlying the generation of complex dynamics. In particular, we believe it would be of interest, for the proposed model, to derive the normal forms of the resonant interaction, both in the case of 1D and 2D domains and investigate through the formalism of the amplitude equations, the phase instabilities which originate the chaotic dynamics [61]. These subjects will be investigated in a forthcoming paper.

ACKNOWLEDGMENTS

We thank the anonymous referees for their comments and suggestions that helped to significantly improve the paper. The authors acknowledge the financial support of GNFM-INdAM.

[1] A. De Wit, D. Lima, G. Dewel, and P. Borckmans, Phys. Rev. E **54**, 261 (1996).
[2] S. Bose, P. Rodin, and E. Schöll, Phys. Rev. E **62**, 1778 (2000).
[3] L. Yang, M. Dolnik, A. Zhabotinsky, and I. Epstein, J. Chem. Phys. **117**, 7259 (2002).
[4] L. Yang, A. M. Zhabotinsky, and I. R. Epstein, Phys. Rev. Lett. **92**, 198303 (2004).
[5] A. Kaminaga, V. K. Vanag, and I. R. Epstein, J. Chem. Phys. **122**, 174706 (2005).
[6] M. Banerjee and S. Banerjee, Math. Biosci. **236**, 64 (2012).
[7] I. Berenstein and Carballido-Landeira, Chaos **27**, 013116 (2017).
[8] A. De Wit, Adv. Chem. Phys. **109**, 435 (1999).
[9] G. Dewel, A. De Wit, S. Métens, J. Verdasca, and P. Borckmans, Phys. Scr. T **67**, 51 (1996).
[10] M. Meixner, A. De Wit, S. Bose, and E. Schöll, Phys. Rev. E **55**, 6690 (1997).
[11] L. Yang, M. Dolnik, A. Zhabotinsky, and I. Epstein, Chaos **16** (2006).
[12] M. Stolyarov, V. Romanov, and E. Volkov, Phys. Rev. E **54**, 163 (1996).
[13] L. Yang and I. R. Epstein, Phys. Rev. Lett. **90**, 178303 (2003).
[14] X.-Z. Li, Z.-G. Bai, Y. Li, and K. Zhao, Mod. Phys. Lett. B **30**, 1650085 (2016).
[15] R. Anguelov and S. Stoltz, Math. Comput. Simulat. **133**, 39 (2017).
[16] E. Tulumello, M. Lombardo, and M. Sammartino, Acta Appl. Math. **132**, 621 (2014).
[17] S. Petrovskii and H. Malchow, Math. Comput. Modell. **29**, 49 (1999).
[18] S. Petrovskii and H. Malchow, Theor. Pop. Biol. **59**, 157 (2001).
[19] A. Medvinsky, S. Petrovskii, I. Tikhonova, H. Malchow, and B.-L. Li, SIAM Rev. **44**, 311 (2002).
[20] W. Wang, Q.-X. Liu, and Z. Jin, Phys. Rev. E **75**, 051913 (2007).
[21] M. Baurmann, T. Gross, and U. Feudel, J. Theor. Biol. **245**, 220 (2007).
[22] W. Wang, Y. Lin, L. Zhang, F. Rao, and Y. Tan, Commun. Nonlinear Sci. **16**, 2006 (2011).
[23] D. Lima, A. De Wit, G. Dewel, and P. Borckmans, Phys. Rev. E **53**, R1305 (1996).
[24] M. Abdechiri, K. Faez, H. Amindavar, and E. Bilotta, Nonlinear Dyn. **87**, 2597 (2017).
[25] R. Barrio, C. Varea, J. Aragón, and P. Maini, Bull. Math. Biol. **61**, 483 (1999).
[26] R.-T. Liu, S.-S. Liaw, and P. Maini, J. Korean Phys. Soc. **50**, 234 (2007).
[27] J. L. Aragón, R. A. Barrio, T. E. Woolley, R. E. Baker, and P. K. Maini, Phys. Rev. E **86**, 026201 (2012).
[28] A.-W. Li, Z. Jin, L. Li, and J.-Z. Wang, Int. J. Mod. Phys. B **26**, 1250193 (2012).
[29] V. Vanag and I. Epstein, Phys. Rev. E **71**, 066212 (2005).

[30] L. Yang, M. Dolnik, A. M. Zhabotinsky, and I. R. Epstein, Phys. Rev. Lett. **88**, 208303 (2002).
[31] Y. Logvin, T. Ackemann, and W. Lange, Europhys. Lett. **38**, 583 (1997).
[32] Y. Logvin and T. Ackemann, Phys. Rev. E **58**, 1654 (1998).
[33] A. Sih, Am. Nat. **123**, 143 (1984).
[34] N. Shigesada, K. Kawasaki, and E. Teramoto, J. Theor. Biol. **79**, 83 (1979).
[35] I. Aranson and L. Tsimring, Phys. Rev. E **65**, 061303 (2002).
[36] G. Galiano, Comput. Math. Appl. **64**, 1927 (2012).
[37] G. Gambino, M. C. Lombardo, M. Sammartino, and V. Sciacca, Phys. Rev. E **88**, 042925 (2013).
[38] G. Galiano and V. Selgas, Nonlinear Anal.: Real World Appl. **18**, 34 (2014).
[39] G. Gambino, M. C. Lombardo, and M. Sammartino, Acta Appl. Math. **132**, 283 (2014).
[40] M. Bendahmane, R. Ruiz-Baier, and C. Tian, J. Math. Biol. **72**, 1441 (2016).
[41] M. Lombardo, R. Barresi, E. Bilotta, F. Gargano, P. Pantano, and M. Sammartino, J. Math. Biol. **75**, 373 (2017).
[42] E. Zemskov, M. Tsyganov, and W. Horsthemke, Phys. Rev. E **95**, 012203 (2017).
[43] M. Pascual, Proc. R. Soc. B **251**, 1 (1993).
[44] R. Cantrell and C. Cosner, J. Math. Biol. **37**, 103 (1998).
[45] Y. Du and J. Shi, Trans. Am. Math. Soc. **359**, 4557 (2007).
[46] A. Morozov, S. Petrovskii, and B.-L. Li, Proc. R. Soc. B **271**, 1407 (2004).
[47] A. Morozov, S. Petrovskii, and B.-L. Li, J. Theor. Biol. **238**, 18 (2006).
[48] Y. Cai, M. Banerjee, Y. Kang, and W. Wang, Math. Biosci. Eng. **11**, 1247 (2014).
[49] J. Sherratt, M. Lewis, and A. Fowler, Proc. Natl. Acad. Sci. USA **92**, 2524 (1995).
[50] J. Sherratt, B. Eagan, and M. Lewis, Philos. Trans. R. Soc. London B **352**, 21 (1997).
[51] R. Wackerbauer and K. Showalter, Phys. Rev. Lett. **91**, 174103 (2003).
[52] D. Stahlke and R. Wackerbauer, Phys. Rev. E **80**, 056211 (2009).
[53] S. M. Houghton, E. Knobloch, S. M. Tobias, and M. R. E. Proctor, Phys. Lett., Sect. A **374**, 2030 (2010).
[54] I. Berenstein and C. Beta, J. Chem. Phys. **136**, 034903 (2012).
[55] I. Berenstein and Y. De Decker, Chaos **24**, 043109 (2014).
[56] D. Das, Phys. Rev. E **92**, 052914 (2015).
[57] H. Hartle and R. Wackerbauer, Phys. Rev. E **96**, 032223 (2017).
[58] K. Sugimura and H. Kori, Phys. Rev. E **92**, 062915 (2015).
[59] G. Gambino, M. Lombardo, and M. Sammartino, Nonlinear Anal. Real World Appl. **14**, 1755 (2013).
[60] B. Bozzini, G. Gambino, D. Lacitignola, S. Lupo, M. Sammartino, and I. Sgura, Comput. Math. Appl. **70**, 1948 (2015).
[61] M. Cheng and H.-C. Chang, Phys. Fluids A **4**, 505 (1992).